Impurity behavior in JET-ILW plasmas fuelled with gas and/or with pellets: a comparative study with the transport code COREDIV

G. Telesca[1], I. Ivanova-Stanik[1], Ch. Perez von Thun[1], S. Aleiferis[2], S. Brezinsek[3], A. Chomiczewska[1], A. Huber[3], E. Kowalska-Strzeciwilk[1], E. Pawelec[4], M. Sertoli[5], R. Zagórski[6]and JET contributors*

EUROfusion Consortium, JET, Culham Science Centre, Abingdon, OX14 3DB,UK
[1]*Institute of Plasma Physics and Laser Microfusion, Warsaw, Poland*
[2]*Institute for Nuclear and Radiological Science and Technology, Safety and Energy, NCSR Demokritos, 15310 Agia Paraskevi, Greece*
[3]*Institut fuer Energie-und Klimaforschung-Plasmaphysik Foschungszentrum Juelich GmbH,Juelich, Germany*
[4]*Institute of Physics, University of Opole, 45-052 Opole, Poland*
[5]*Culham Centre for Fusion Energy, Culham Science Centre, Culham, UK*
[6]*National Centre for Nuclear Research, Pl-05-400, Otwock, Poland*

Email: giuseppe.telesca@ifpilm.pl

Abstract

This study deals with the comparison of impurity behaviour in pellet and gas fuelled JET-ILW pulses with the aim of finding the mechanisms leading to the generally observed higher high-Z impurity concentration in pellet fuelled plasmas. Analysis of the experimental data pertaining to pulses at different plasma currents, different input power and different electron densities is integrated by numerical modelling with the self-consistent fluid transport code COREDIV. Experimentally, and numerically, the ratio between the radiated power in the divertor and the total one – proportional to the ratio of the density at the strike point to the volume average one - is found to be the critical parameter determining impurity accumulation. The higher this value the lower the impurity density in the plasma core. Together with a little higher core impurity residence time, the modelling results indicate that the modest divertor screening for the pellet fuelled pulses at low electron flow – characterized by low electron density at the strike point and low perpendicular transport in the SOL– leads to divertor impurity leakage and higher impurity fluxes through the separatrix to the confined plasma, in agreement with theory.

*See the author list in E. Joffrin et al., 2019 Nucl. Fusion 59 11202

1.Introduction

In support of establishing an integrated ITER scenario and also in preparation of the next DT JET-ILW [1] campaign a series of experiments at different plasma currents and different auxiliary heating power levels have been recently carried out at JET in which fuelling by gas puff and pellets are compared with respect to the energy confinement and impurity behaviour properties [2]. In fact, pellet injection might overcome the expected insufficient gas puff fuelling efficiency for the ITER plasmas and might also represent a tool to control the ELM frequency. Moreover, in previous JET-ILW experiments at very high input power [3] it has been observed that the energy confinement increases with pellet fuelling (or pacing) in comparison with gas puffing rendering pellet fuelling quite an attractive scenario for thermonuclear plasmas.

Independently of these relevant high confinement experimental results, the aspect of pellet fuelling we are interested in relies on the purity of the associated plasmas. In fact, considering that, in general, the plasma purity is observed to be higher for gas fuelled plasmas, a major concern refers to the possibility of high-Z impurity accumulation, and related core radiative losses, for pellet fuelled plasmas. This work is focused on the comparison of the two fuelling methods with respect to high-Z impurity density and radiation, with the aim of identifying some basic possible differences in the mechanisms of impurity transport. Among all the pulses performed for this comparison during a recent JET-ILW experimental campaign, which extend to a large variety of experiments characterized by different densities, input powers, confinements and plasma currents, we have selected for this study one couple of pulses at I_p= 2.1 MA and B_T= 2 T and, more specifically, a series of seven pulses (three with gas puff only, four with reduced gas puff + pellets) at I_p= 3 MA, B_t = 2.85 T with average electron density $<n_e>$ about 6.4 x 10^{19} e/m^3 and total input power about 25 MW (21 MW NBI + 4 MW ICRF heating). The peculiarity of these seven pulses relies in the value of their stored energy, which is very similar for gas puff only and pulses with pellets. This renders the study of impurity behaviour significantly simpler since for all the seven pulses the electron density and temperature profiles are nearly identical. The stored thermal energy, W_{th} and associated confinement factor, H_{98}, as well as Z_{eff} are about 6.4 MJ, 0.83 and 1.4 respectively, and the pedestal densities are also very similar, within 5 percent. In contrast, the total radiated power, P_{tot}^{rad}, the ratio of the radiated power in the divertor to the total one, $P_{DIV}^{rad}/P_{tot}^{rad}$, and high-Z impurity concentrations can be significantly different. (Please, note that P_{DIV}^{rad} is used to indicate the level of the radiated power below the vertical coordinate value = -1 m [4].

Unfortunately, for the seven pulses at I_p = 3 MA the ELM behaviour of the pulses with gas only (Type I ELMs) is quite different from those with pellets (a mixture of Type I, Type III and compound ELMs, (see Ref. 2), rendering a useless exercise trying any estimation of the effects of the ELM frequency, f_{ELM}, on the impurity residence time in the two scenarios (see also Sect. 3 and Sect.4). Indeed, ELMs are the main cause of impurity production as well as of flushing out [5-7]. Although f_{ELM} increases with increasing the total electron flow and this is generally assumed to account for the decrease both of the impurity residence time [8] and of the energy confinement time, for the pellet pulses here considered the impurity flushing out action of ELMs cannot be easily quantified. What can be quantified is the time-averaged value of few parameters: the only clear data refer to the time-averaged higher P_{tot}^{rad}, to the higher high-Z impurity concentration and to the lower $P_{DIV}^{rad}/P_{tot}^{rad}$ in the case of pellet fuelling or pacing. Considering the similarity of the core electron temperature and density profiles, we have assumed, as a preliminary working hypothesis, core impurity transport to be *nearly* the same - on the average (see Sect. 3.2) - in the two fuelling methods, with anomalous impurity transport set to be equal to the main particles, see Sect 2 and Ref. [9].

Although it is widely accepted that impurity transport is mostly determined by the time-dependent ELM behaviour, in this study the comparison between time-averaged experimental signals and numerical reconstruction is performed by the results of the steady-state COREDIV transport code. Use of this method does not imply disavowal of the central role of ELMs in determining the impurity sources, sinks and transport [10], but it is made as a search for other possible mechanisms capable to account, at least partly, for the observed higher tungsten concentration in pellet fuelled plasmas. In Ref. [11] it is shown that the W erosion source increases with f_{ELM}, reaches its maximum at about 55 Hz and then decreases with f_{ELM}. While the W content increases with the source at low frequency, beyond 40 Hz there is a tendency for saturation or even descent, which is probably due to flushing of W from the confinement volume by the action of the ELMs [12]. One has to consider, however, that f_{ELM} is not an independent variable, but most often depends on the gas fuelling rate [8,13] or on the fuelling capability of pellets[14], which are related also to the increase/decrease in divertor and SOL density.

Taking the experimental time-average values (about one second, a few energy confinement times) of P_{tot}^{rad}, $P_{DIV}^{rad}/P_{tot}^{rad}$, Z_{eff}, and high-Z impurity concentrations and using the steady-state version of the transport code COREDIV we have tried to reconstruct numerically the experimental data by keeping in the code *nearly* the same core impurity transport coefficients for all the considered seven pulses (see Sect.3). COREDIV is a fluid transport code which couples self-consistently - with respect to the energy, particles and radiation - the 1D core model with the 2D SOL module in such a way that any change in the SOL causes consistent changes in the core and vice versa. This is described in Sect. 2, while in Sect. 3 the experimental data are presented together with the comparison with the numerical results. Discussion of the results is made in Sect. 4 and conclusions are drawn in Sect. 5 with a summary of this work.

2. The COREDIV model

We have used the COREDIV code [15], self-consistent with respect to the core-SOL as well as to impurities-main plasma. In spite of some simplifications, especially in the SOL model (slab geometry and model of the neutrals), the exchange of information between the core (1D) and the SOL (2D) module renders this code quite useful when, as in the case of the JET ILW, the interaction SOL-core is crucial.

In the core, given as code input the volume average electron density $\langle n_e \rangle$, the 1D radial transport equations for bulk ions, for each ionization state of impurity ions and for the electron and ion temperature are solved. The electron and ion energy fluxes are defined by the local transport model proposed in Ref. [16] which reproduces a prescribed energy confinement law. In particular, the anomalous heat conductivity is given by the expression $\chi_{e,i} = C_{e,i} * a^2/\tau_E * F(r)$ where r is the radial coordinate, a is the plasma radius, τ_E is the energy confinement time defined by the ELMy H-mode scaling law and the coefficient ($C_e = C_i$) is adjusted to have agreement between calculated and experimental confinement times. The parabolic-like profile function $F(r)$, which may slightly change from run to run in order to match with the actual profiles of the experimental pulse to be modelled, can be modified at the plasma edge to provide for a transport barrier of chosen level. The main plasma ion density is given by the solution of the radial diffusion equation with diffusion coefficients generally $D_i = D_e = 0.1\ \chi_e$, as in Ref.[16]. In Sect. 4 a numerical scan of D_e/χ_e is made with the purpose of changing the impurity residence time, but this does not affect the density profile of the main plasma since the solution of the diffusion equation for the main plasma is largely independent of the exact value of D_e/χ_e. Indeed, a change in D_e/χ_e causes a consistent change in the source term, since the average electron

density is a COREDIV input. For the auxiliary heating, parabolic-like deposition profile is assumed $P_{aux}(r) = P_0 (1-r^2/a^2)^y$ where y is in the range 1.5-3, depending on the quality of the auxiliary heating, NBI or/and ICRF. In conclusion: once the power deposition profile, the confinement time τ_E and the profile function $F(r)$ are assigned, the electron temperature and density profiles are unambiguously determined. For the pulses considered in this study y=2. Impurity diffusion coefficient is set to be equal to that of the main ions and the anomalous impurity pinch, which is a code input, is set to zero for these pulses [9], see Sect.3.
In the SOL we use the 2D boundary layer code EPIT [17], which is primarily based on Braginskii-like equations [18], for the background plasma and on rate equations for each ionization state of each impurity species. An analytical description of the neutrals is used, based on a simple diffusive model. COREDIV takes into account the plasma (D, Be and seeded impurities) recycling in the divertor as well as the sputtering processes at the target plates including deuterium sputtering, self-sputtering and sputtering due to seeded impurities. (For deuterium and neon sputtering and tungsten self-sputtering the yields given in Refs. [19, 20] are used). While the W fluxes are computed self-consistently, those of Be and Ni are given as code inputs (see Sect. 3). The recycling coefficient is an external parameter which in COREDIV depends on the level of the electron density at the separatrix, n_{e_sep}, given as an input, and increases with increasing n_{e_sep}.

A simple slab geometry (poloidal and radial directions) with classical parallel transport and anomalous radial transport ($D_{SOL} = \chi_i = 0.5\ \chi_e$, where χ_e ranges typically 0.4-1 m^2/s), is used and the impurity fluxes and radiation losses by impurity ions are calculated fully self-consistently. Although the values of the transport coefficients in the SOL are generally quite comparable to those at the separatrix, in the present simulations the value of D_{SOL} is set arbitrarily (in the range 0.1-0.3 m^2/s) in order to match with the core-SOL distribution of the radiated power (see Sect.3). All the equations are solved only from the midplane to the divertor plate, assuming inner-outer symmetry of the problem. This implies that the experimental in–out asymmetries, observed especially at high density-high radiation level, are not reproduced in COREDIV results. However, for all the different situations examined so far (with carbon plates and with the ILW, and with different seeding levels [21]) the COREDIV numerical reconstructed total radiation in the SOL matches well with the total experimentally measured SOL radiation, indicating that for JET conditions the edge-core COREDIV model can describe the global trend of this important quantity. The coupling between the core and the SOL is made by imposing continuity of energy and particle fluxes as well as of particle densities and temperatures at the separatrix. The computed fluxes from the core are used as boundary condition for the SOL plasma. In turn, the values of temperatures and of densities calculated in the SOL are used as boundary conditions for the core module

3. Experimental data and numerical results

For the series of seven pulses at I_p = 3 MA there are no data for Be fluxes as well as concentrations (see below), but judging from the similarity of Z_{eff} in all the seven pulses one can assume that the Be concentrations are also similar. Indeed Z_{eff} is mainly determined by Be in JET-ILW [22]. In the COREDIV simulations here reported Be and Ni fluxes are code inputs (see Sect. 2) and it has been set $\phi_{Be} = 1.5\ x10^{21}$ p/s and $\phi_{Be} = 2.0\ x10^{21}$ p/s for pellets and gas puff pulses, respectively, taking into account the higher plasma-wall interaction of gas puff pulses, consistently with the higher SOL density. This results in similar Z_{eff} for pellet and gas puff pulses, as in the experiments. For Ni it is set $\phi_{Ni} = 2.0\ x10^{19}$ p/s both for pellets and gas puff. Considering that in this series of seven pulses the input power and the stored energy are quite similar as well as the pedestal structure [2], the significant difference in P_{tot}^{rad} , in $P_{DIV}^{rad}/P_{tot}^{rad}$ and in high-Z impurity concentration might also arise from differences in the SOL transport. Unfortunately, due to the magnetic configuration (the so-called corner-corner configuration [4]) for these pulses it was not possible a measure of the electron temperature and density as well as of some spectral lines near the OSP.

In the following it will be reported the W concentration, c_W, as experimentally derived from the Soft- X- Ray, SXR, diagnostic. It is worth mentioning that this is a rather complex measure. Indeed, to obtain consistent results the analysis of SXR has to be integrated with the analysis of the Vacuum Ultra Violet, VUV, spectra and bolometric signals [23,24].

3.2 Two pulses at I_p= 2.1 MA

One couple of pulses very similar in input power (about 14.3 MW) and in $<n_e>$ (about $5.3 \times 10^{19}\ m^{-3}$) at I_p= 2.1 MA and B_T = 2.0 T one with pellets only the other with gas puff + pellets have been performed with a magnetic configuration that has allowed the measurement of the electron temperature and density at the outer plate to be taken as well as that of the WI and WVII line intensities. For these two pulses Langmuir Probes, LP, (Fig. 1) indicate at the outer target about a factor of two lower temperature and about a factor of two higher density for the pulse with gas puff + pellets (95718, total nominal electron flow= 2.73 x 10^{22} e/s) in comparison to pellets only (95717, total nominal electron flow=1.28 x 10^{22} e/s). (It is worth mentioning that the values of the total nominal electron flow reported throughout this paper are affected by some uncertainties due to the different locations of the gas puff inlet valves used in different pulses, with related different effective fuelling rates [2]). Fig.2 shows that the W line emissions in the divertor at λ = 400.8 nm for W I and at λ = 26.1 nm for W VII are not higher for the pulse with pellet only than for the pulse with gas puff+pellets , while from SXR diagnostic, the W concentration, c_W, is indeed higher : c_W = 4.1 x 10^{-5} for pellet only and c_W= 2.6 x10^{-5} for the other, in agreement with bolometric data. Indeed, from bolometry the time averaged (49 s< t< 50.5s) P_{tot}^{rad} = 5.18 MW for the pulse gas+pellets and P_{tot}^{rad} = 6.0 MW for pellet only, while the ratio $P_{DIV}^{rad}/P_{tot}^{rad}$ is higher for the gas+ pellets as compared to pellets only, about 0.28 and 0.20, respectively.

These data indicate that for these two pulses $P_{DIV}^{rad}/P_{tot}^{rad}$ reflects, and goes together with, the ratio of the density at the strike point to the volume average one, n_{e_SP}/<ne>, and that the W transport might change significantly when the divertor densities are different, even for pulses with the same $\langle n_e \rangle$, same input power and same H_{98}. Although the pulse with gas puff + pellets shows higher f_{ELM} as well as higher BII line intensity than that with pellets only, see Fig.3, the main parameters of these two pulses have been successfully reproduced in a steady-state simulation using the same core inputs. Only the Be fluxes, according to the experimental data, are set to be a little higher for the gas puff pulse than for the pellet one Φ_{Be}= 2.0 x 10^{21} p/s and Φ_{Be}= 1.5 x 10^{21} p/s, respectively. This result has been achieved by setting as code inputs, see Sect. 2, different perpendicular particle diffusivity in the SOL (D_{SOL} = 0.25 m^2/s and D_{SOL} = 0.10 m^2/s) and different SOL densities, as in the experimental data, resulting in n_{e_SP} = 2.0 x 10^{20} m^{-3} and n_{e_SP} = 1.3 x 10^{20} m^{-3}, for the gas puff + pellets and pellet only, (please, recall the slab geometry of the SOL in COREDIV, Sect.2). Even though the numerical W fluxes at the target are similar for the two pulses (about 1.5 x 10^{19} p/s) the numerical W core concentrations are different, as they are in the experimental SXR data : c_W = 4.9 x 10^{-5} and c_W = 2.7 x 10^{-5} for the gas puff +pellets and for the pellet only pulse, respectively. This shows that in steady-state numerical COREDIV simulations with the same W fluxes and *similar* core transport (see Sect. 3.2) the value of the SOL density and of D_{SOL} might cause significant differences in the W core concentration.

3.2 Experiments and simulations of the seven pulses at I_p=3 MA.

In Fig.4 some experimental data of the seven pulses are shown together with the corresponding COREDIV results, plotted as a function of the nominal total electron flow. Experimentally, for the pulses with gas puff only the increase in puffing rate from $\Phi_e = 4.9 \times 10^{22}$ e/s to $\Phi_e = 6.8 \times 10^{22}$ e/s leads to the decrease in P_{tot}^{rad} from 10.3 MW to 7.7 MW, accompanied with the increase in the ratio of the radiated power in the divertor to the total one ($P_{DIV}^{rad}/P_{tot}^{rad}$) from 0.194 to 0.265 For the pellet pulses (fuelling or pacing) P_{tot}^{rad} decreases slowly with increasing the electron flow from 11.14 MW to 10.0 MW and $P_{DIV}^{rad}/P_{tot}^{rad}$ is lower than with gas puff only, in the range 0.149 - 0.179. With respect to high-Z impurities the VUV and SXR diagnostics show a definite difference between the two fuelling methods. For the gas puff only, the W concentration in the plasma core, c_W, decreases monotonically from 0.49×10^{-4} to 0.3×10^{-4} with increasing the puffing rate and for the pellet pulses from 0.64×10^{-4} to 0.49×10^{-4}. Similar trend is observed for Ni concentration. It should be noted that the experimental parameters of the two pellet pulses at the highest nominal electron flows are quite similar to those of the pulse with gas puff only at the lowest electron flow. This might suggest that the nominal total electron flow, and the related SOL density, is the common denominator what the average P_{tot}^{rad}, $P_{DIV}^{rad}/P_{tot}^{rad}$ and c_W are concerned, independently of the fuelling method.

To give an example, in Fig.5 it is shown the bolometric tomographic reconstruction for the pulse at the highest electron flow for gas puff (94749, $\phi_e = 6.8 \times 10^{22}$ e/s) and for the pellet pulse at the lowest electron flow 94754 $\phi_e = 2.2 \times 10^{22}$ e/s). These two plots show quite clearly the difference in radiation pattern of the two pulses which are characterised by P_{tot}^{rad} = 7.7 MW and P_{tot}^{rad} = 11.1 MW and by $P_{DIV}^{rad}/P_{tot}^{rad}$ = 0.265 and $P_{DIV}^{rad}/P_{tot}^{rad}$ = 0.149 for the gas puff and pellet pulses, respectively. The experimental and the numerical reconstructed electron temperature and density profiles in the plasma core for these two pulses are shown in Fig. 6. Note that the profiles of these two pulses are the most different among the whole series. The profiles of the remaining five pulses are nearly identical to those of pulse 94749. The other numerical parameters, to be compared to the experimental ones, are: P_{tot}^{rad} = 8 MW and = 10.58 MW, $c_W = 0.38 \times 10^{-4}$and 0.61×10^{-4}, $c_{Ni} = 1.7 \times 10^{-4}$ and 3×10^{-4}, $P_{DIV}^{rad}/P_{tot}^{rad}$ = 0.30 and = 0.142 for the simulated gas and pellet pulses, respectively. Except for a minor change in confinement factor (H_{98}= 0.81 and 0.84), only two inputs have been changed in the runs related to each of these two pulses, as done for the two pulses at I_p= 2.1 MA: the density at the target plate and the particle perpendicular diffusion coefficient in the SOL, D_{SOL}. The target plate density was set to be lower for the pulse with pellets leading to $n_{e\_SP}/\langle ne \rangle = 3.3$ for the pellets and to

n_{e_SP}/<ne> = 4.8 for the pulse with gas puff, where n_{e_SP} is the electron density at the strike point, and D_{SOL} was set to be 0.10 m^2/s for the pulse with pellets and 0.23 m^2/s for the pulse with gas puff. Changing only one of these two inputs was not sufficient to satisfactorily reproduce the main parameters of these two pulses. The numerical W fluxes are not much different for these two pulses, Φ_W = 3.0 x 10^{19} p/s for the pellet pulse and Φ_W = 2.6 x 10^{19} p/s for the gas pulse. In fact, the higher SOL electron temperature for the pellet pulse tends to compensate for the lower density, what the total W sputtering is concerned in the relevant temperature and density range.

It has to be pointed out that for pulses with the same density, same input power and same stored energy, but different radiation level, the core energy and particle transport coefficients are not exactly the same but only *similar*, both in the experiment and simulations. Indeed, same input power and same stored energy and higher core radiation losses of the pellet pulse imply lower energy transport coefficients. In this case the transport coefficients for the pellet pulse are about 15 percent lower than for the gas one, i.e. the numerical factor $C_{i,e}$ changes from 0.42 to 0.36, see Sect. 2.

4. Dicussion.

Independently of the different height and quite different behaviour of the ELMs in the series of seven pulses, f_{ELM} is in the range 30-60 Hz for pellets and 38-57 Hz for gas puff. Although the analysis of ELM behaviour is not the main subject of this work, it should be mentioned, just to give an example, that the ELM behaviour of the pellet pulse at the highest total electron flow is quite different from that of the gas puff pulse at the lowest electron flow (see Fig.7), in spite of similar total electron flow, and time-averaged P_{tot}^{rad}, $P_{DIV}^{rad}/P_{tot}^{rad}$ and W concentration, see previous section. Indeed, from a steady-state point of view these two pulses are modelled (within the error bar of the measurements) with the same inputs: n_{e_SP} = 2.7x10^{20} $m^{-3}$and D_{SOL}= 0.14 m^2/s.

On the other hand P_{tot}^{rad} and c_W (and P_{core}^{rad}) are significantly higher in the pellet pulse at the lowest electron flow as compared to the gas one at the highest flow rate while $P_{DIV}^{rad}/P_{tot}^{rad}$ is much lower. In order to try to clarifying if this difference arises from the impurity core transport only or also from other mechanisms a COREDIV numerical test has been performed. Keeping all the inputs unchanged we have increased, step by step, only the impurity core diffusivity for the original pulse at the lowest electron flow (pellet) up to the level the c_W decreases from 0.61 x 10^{-4} to the simulated value (0.38 x 10^{-4}) of the pulse at the highest flow (gas). One needs to increase the core diffusivity by a factor of 8 to match the two W concentrations, as seen in Fig. 8 where c_W and T_{i_SP} (ion temperature at the strike point) are plotted vs particle diffusivity. Since in the simulations P_{DIV}^{rad} remains low (about 1.55 MW) also at the highest core diffusivity while the bulk radiation decreases from the (experimental and simulated) value of 9.4 MW to the simulated value of 5.8 MW at the highest diffusivity, the power to the plate increases significantly (about 16 MW, considering also charge exchange losses) with respect to the real pellet pulse (about 12 MW) resulting in the increase of T_{i_SP} from 33 eV to 55 eV. Please, note that the mentioned factor of 8 is the result of two mechanisms: the decrease of the impurity confinement time with D/χ and the simultaneous increase of the impurity fluxes into the confined plasma, caused by the increase in the divertor temperature. This numerical test suggests that, at least what the steady-state reconstruction is concerned, core transport should change dramatically to be the only and dominant mechanism for the observed decrease of high-Z impurity concentrations in gas puff pulses.

For completeness, it is here reported the situation of the only couple of pulses - one with pellets the other with gas puff - which show the same f_{ELM}. For these two pulses there are some uncertainties in the absolute value of c_W and of the W I and W VII line intensities, possibly related to a lack of stationarity in the magnetic configuration, which changes three times during the flat top. The two pulses are at I_p= 2.1 MA and B_t = 2.0 T, P_{aux} = 17.5 MW one with gas puff only (96177, H_{98}= 1.12, electron flow= 3.2x 10^{22} e/s), the other with pellets + low level gas puff (96175, H_{98}=1.04, total electron flow = 1.28 x10^{22} e/s +1.13 x10^{22} e/s). In the time interval 52.5 s < t < 53.5 s the magnetic configuration is rather similar to the corner-corner configuration what the position of the OSP is concerned, and the Type I ELM behaviour is nearly identical for these two pulses, same height and same frequency (f_{ELM} =70Hz). In spite of the higher electron flow of the pulse with gas only the electron density, $\langle n_e \rangle$=3.8 x 10^{19} m^{-3}, is lower than that of the pellet pulse, $\langle n_e \rangle$=4.3 x 10^{19} m^{-3}, as it is P_{tot}^{rad} (4.2 MW and 4.7 MW, respectively), but $P_{DIV}^{rad}/P_{tot}^{rad}$ (= 0.37 and 0.30, respectively) is higher as can be seen from the tomographic reconstruction in Fig 9. Within the uncertainties in the absolute values, the experimentally derived c_W and the measured WI and W VII line intensities are practically identical in these two pulses, see Fig. 10, as are the COREDIV reconstructed c_W = 0.69 10^{-4} and the W flux at the plate Φ_W = 2.1 x 10^{19} p/s. The code inputs for these two simulations are D_{SOL}=0.15 m^2/s and D_{SOL}=0.11 m^2/s and the electron density at the target are n_{e_SP} = 2.10 x 10^{20} 1/m^3

and n_{e_SP} = 2.0 x 10^{20} 1/m^3 for the gas puff and pellet pulse respectively. Taking into account the difference in <n_e> of the two pulses this implies a lower W density for the gas puff pulse, which might suggests again that f_{ELM} and core confinement are not the only mechanisms responsible for the tendency of impurity accumulation for the pellet pulses, but also the lower electron flow and the lower perpendicular SOL transport matter.

In fact, from COREDIV simulations for the pulses here considered the ratio of the total W flux at the target to that at the separatrix is higher by up to 25 percent for the gas puff pulses with respect to those with pellets, indicating a better divertor impurity screening.

The implications for impurity transport of different SOL densities and D_{SOL} for the pulses of our interest have been analysed by the results of the COREDIV code. In the most common situations good impurity retention capability of the divertor is determined by the balance of the collisional drag force and the ion gradient thermal force: the collisional drag should be stronger than the thermal force [25] in the region upstream of the impurity release area [26]. An order of magnitude comparison between the frictional drag and the thermal forces shows [27] that divertor impurity retention occurs if $M_p > \lambda_{DD}/\lambda_T$ where M_p is the local Mach number, λ_{DD} is the deuteron mean free path and λ_T is the temperature gradient length. From the results of COREDIV it is seen that, in general, the ratio λ_{DD}/λ_T decreases with increasing $P_{DIV}^{rad}/P_{tot}^{rad}$ (i.e. with increasing $n_{e\text{-}pl}$/<ne>) mostly due to the reduction of the deuteron mean free path, while the variations of the temperature gradient length are relatively modest for the series of seven pulses here considered. Since M_p is in the range 0.3- 0.5 the divertor retention results to be more efficient for the pulses at high $P_{DIV}^{rad}/P_{tot}^{rad}$. For the pulse at the highest gas puffing rate we obtain M_D= 0.3 and λ_{DD}/λ_T = 1.2 x 10^{-2} while for the pellet pulse at the lowest total electron flow M_D= 0.4 and λ_{DD}/λ_T = 4.6 x 10^{-2}. These values are derived from the steady-state numerical SOL profiles near the OSP where the gradients are calculated along the separatrix. Even thought these absolute values are only indicative since they may change changing the field line along which they are calculated and also due to the simplified geometry of the SOL module of COREDIV, the trend is quite clear and reflects the increase of the frictional drag with increasing the electron density [28]. This holds in the range of densities and input powers of the considered pulses. In high recycling regimes the ion temperature gradient near the divertor plates can be much higher with related decrease of λ_T.

In conclusion, the analysis of the experimental data as well as that of the steady-state COREDIV results shows that the observed tendency of pellet pulses at low electron flow to be prone to high-Z impurity accumulation is correlated both with the increase of particle residence time, possibly dependent on higher plasma bulk rotation (3) and with reduced divertor screening. Even though it remains an open question if these two mechanisms are correlated, from the operational point of view pellet fuelling at high electron flow appears to be beneficial to limit the high-Z impurity concentration and core radiative losses.

5. Summary

A couple of pulses at I_p=2.1 MA, one pulse with pellet the other with gas puff, and a series of seven pulses (three with gas puff, four with pellets) at I_p= 3 MA have been analysed and numerically reconstructed with the steady-state fluid code COREDIV. The pulses at I_p=2.1 MA are performed in a magnetic configuration which allows the LPs and spectroscopic data to be taken at the OSP while for the others these data couldn't be taken, due a different magnetic configuration. The two pulses at I_p= 2.1MA show that while the WI and WII line intensities in the divertor are not higher for the pellet pulse as compared to the gas puff one the c_W is higher in the pulse with pellets. The two pulses can be numerically simulated (comparing the time-averaged values of the main plasma parameters with the numerical results) using, as code inputs, lower electron density and lower perpendicular diffusion coefficient in the SOL for the pellet pulse, while keeping unchanged impurity core transport.

The considered pulses of the I_p=3 MA series display quite similar stored energy and nearly identical temperature and density core profiles rendering realistic the modelling hypothesis that core impurity transport is nearly the same for pellet and gas puff pulses, in spite of different ELM behaviour. In absence of LP data the ratio of the radiated power in the divertor to the total one $P_{DIV}^{rad}/P_{tot}^{rad}$ is taken as a measure of the ratio of the electron density at the strike point to the volume average one. Also for this series of pulses numerical modelling was successfully accomplished by simply reducing for the pellet pulses the electron density and the perpendicular particle diffusion coefficient in the SOL. On the other hand, a numerical scan of the impurity diffusion coefficient in the core shows that only an unrealistically high difference in core impurity transport would - if considered as the only mechanism- satisfactorily account for the difference in W concentration in the two scenarios. COREDIV results indicate that the generally observed lower divertor density in pellet pulses causes the increase of impurity leakage with related increase of the impurity fluxes in the confined plasma, in qualitative agreement with theoretical findings. The experimental observations and the COREDIV results lead to the conclusion that the tendency of pellet pulses at low electron flow to display higher c_W is to be attributed partly to reduced core impurity transport and partly to reduced divertor impurity screening. To fully clarifying this point, new experiments with pellet fuelling at high electron flow are planned to be performed at JET-ILW in the near future.

Acknowledgements

This work has been carried out within the framework of the EUROfusion Consortium and has received funding from the Euratom research and training programme 2014-2018 and 2019-2020 under grant agreement No 633053. The views and opinions expressed herein do not necessarily reflect those of the European Commission.

This scientific work was supported by the Polish Ministry of Science and Higher Education within the framework of the scientific financial resources in the years 2019 and 2020 allocated for realization of the international co-financed project.

References

[1] G. F. Mattews et al. Journal Nucl. Mater (2012)

[2] Ch. Perez Von Thun et al. " Pellet-gas comparisons with matched ELM frequency of pedestals, SOL, ELMs, impurities and core confinement in JET-ILW" To be presented at the FEC 2020 Conference

[3] H-T. Kim et al. Nucl. Fusion **58** (2018) 036020

[4] G. Telesca et al. NF 2018 Nucl. Fusion **59** (2019) 056026

https://dx.doi.org/10.1088/1741-4326/ab0c47

[5] A. Loarte et al. 2014 Nucl. Fusion **54** 033007

[6] R. Dux et al. Nucl. Fusion **51** (2011) 053002

[7] S. Brezinsek et al. Nucl. Fusion **59** (2019) 096035

[8] C. F. Maggi et al. 2015 Nucl. Fusion **55** 113031

[9] M. Valisa et al. "The role of ELM's and inter-ELM phases in the transport of impurities in JET". 44th EPS Conference on Plasma Physics P4. 174

[10] R. Dux et al. 2009 J. Nucl. Mater**. 390-1 85**

[11] N. Den Harder et al. 2016 Nucl. Fusion **56** 026014

[12] A . Hueber et al., "Erosion and screening of tungsten during inter/intra-ELM periods in the JET-ILW divertor" To be presented at the PSI 2020 Conference

[13] P. Devynck et al. 2016 Plasma Phys. Control. Fusion **58** 125014

[14] T. Puetterich et al. "Tungsten screening and impurity control in JET" 2012, Proceedings of the 24th IAEA Fusion Energy Conf., San Diego, USA, 8 -13 October 2012 (IAEA, Vienna, 2012) Vol. IAEA-CN-197, EX/P 3.1

[15] R. Zagorski et al. 2013 Nucl. Fusion **53** 073030

[16] J. Mandrekas and W.M. Stacey, Nucl. Fusion **35** (1995) 843

[17] R. Zagorski et al. 1996 J. Tech. Phys. **37** 7

[18] S.I. Braginskii, Rev. Plasma Phys. **1** (1965) 205.

[19] Y. Yamamura et al. , Report of the IPP Nagoya, IPPJ-AM-26 (1083)

[20] C. Garcia-Rosales et al., J. Nucl. Mater. 218 (1994) 8-17

[21] G.Telesca et al. 2011, Plasma Phys. Control. Fusion **53** 115002

[22] S. Brezinsek et al., Nucl. Fusion **54** (2014) 103001

[23] A. Czarnecka et al. 2011, Plasma Phys. Control. Fusion **53** 035009

[24] M. Sertoli et al. J. Plasma Phys., (2019), vol. 85, 905850504

[25] Y. Homma et al, Contributions to Plasma Physics, 2018, DOI : 10.1002/ctpp.201700173

[26] P. C. Stangeby and J. D. Elder, Nucl. Fusion **35** (1995) 1391

[27] J. Neuhauser, et al. Nucl. Fusion **24** (1984) 39

[28] H. A. Claassen and H. Repp, Nucl. Fusion **21** (1981) 589

Figure captions

Fig. 1. LP data for pulses 95717 (pellet) and 95718 (gas)

Fig. 2 WI and W VII line intensity for pulses 95717 (pellet) and 95718 (gas)

Fig. 3 Be II line emission for two pulses at I_p= 2.1 MA, 95717 (pellet) -95718 (gas)

Fig. 4. Experimental and simulated P_{tot}^{rad}(a), $P_{DIV}^{rad}/P_{tot}^{rad}$ (b), c_W and c_{Ni} (c) as a function of the nominal total electron flow. Fig. 4 (d) electron density at the target plate and perpendicular SOL diffusion coefficient used in the simulations.

Fig.5 Bolometric reconstruction for pulses 94749 (gas) and 94754 (pellet)

Fig. 6 Simulated COREDIV and experimental HRTS T_e and n_e profiles for pulses 94749 (gas) and 94754 (pellet).

Fig 7 ELM behaviour for pulses 94755 (gas) and 94756 (pellet),

Fig 8 Simulated c_W and $T_{i\text{-}pl}$ for pulse 94754 (originally pellet) as a function of the ratio diffusivity of W/ heath conductivity

Fig. 9 Tomographic reconstruction of the radiated power for pulses 96175 (pellet) and 96177 (gas)

Fig. 10. WI line intensity for pulses 96175 (pellet) and 96177 (gas) as a function of time.

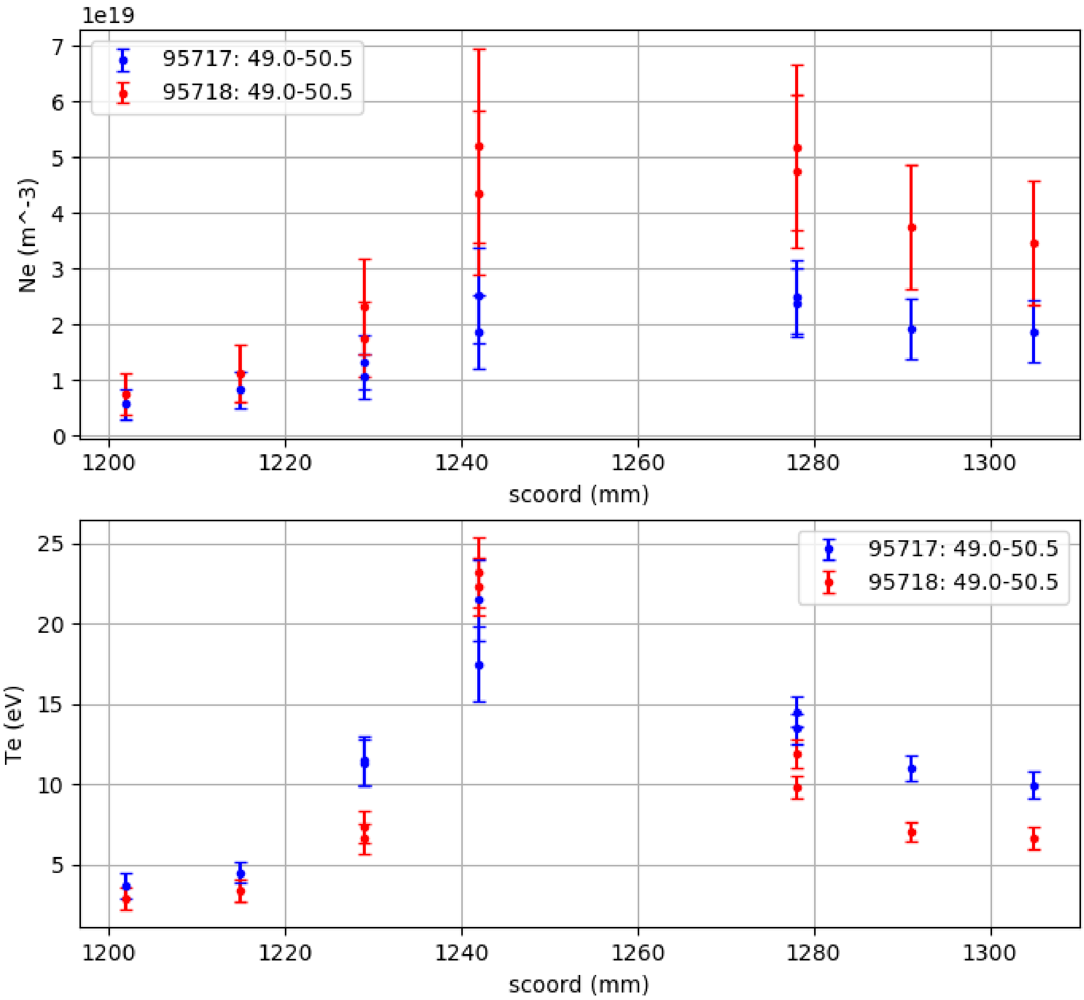
1e19
95717: 49.0-50.5
95718: 49.0-50.5
Ne (m^-3)
scoord (mm)
95717: 49.0-50.5
95718: 49.0-50.5
Te (eV)
scoord (mm)

Fig.1

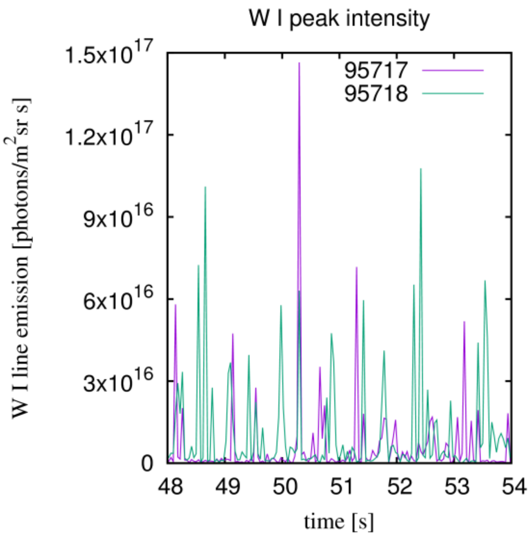

W I peak intensity
W I line emission [photons/m^{2}sr s]
1.5x10^{17}
1.2x10^{17}
9x10^{16}
6x10^{16}
3x10^{16}
0
95717
95718
48
49
50
51
52
53
54
time [s]

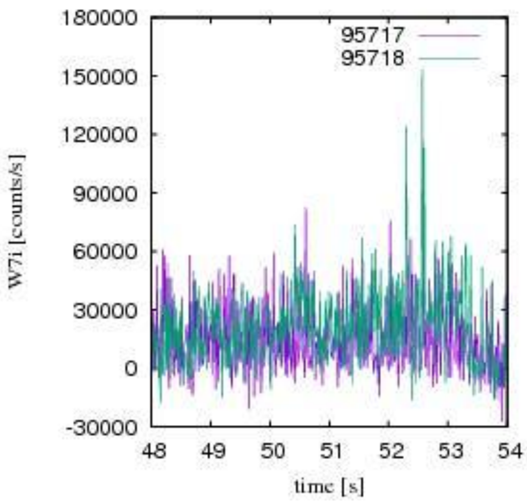

W7i [counts/s]
180000
150000
120000
90000
60000
30000
0
-30000
95717
95718
48
49
50
51
52
53
54
time [s]

Fig. 2

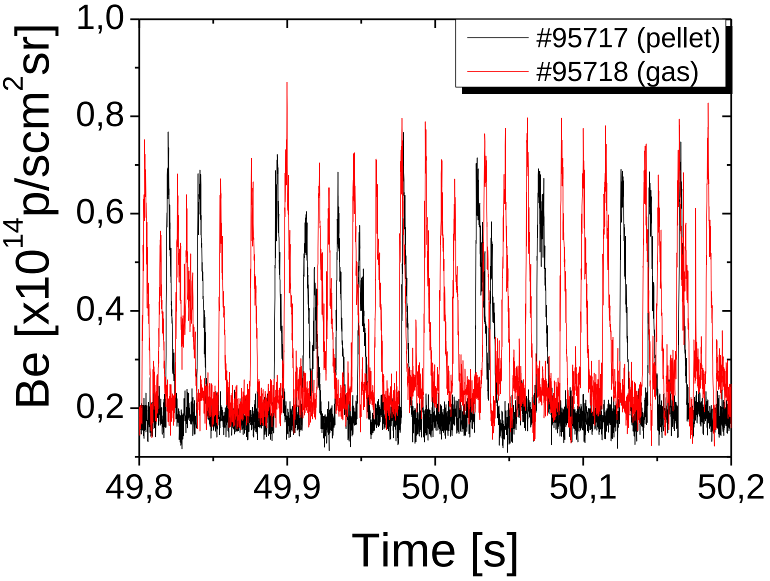
#95717 (pellet)
#95718 (gas)
Be [x10^14 p/scm^2 sr]
1,0
0,8
0,6
0,4
0,2
49,8
49,9
50,0
50,1
50,2
Time [s]

Fig. 3

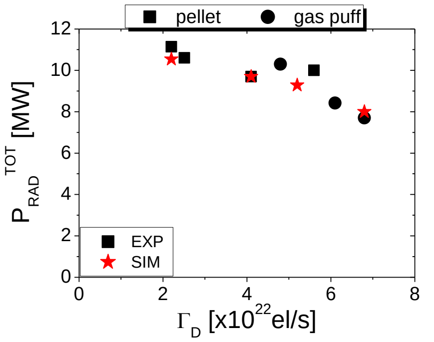

Fig. 4a

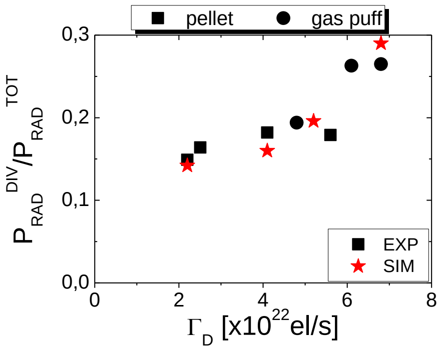

Fig.4b

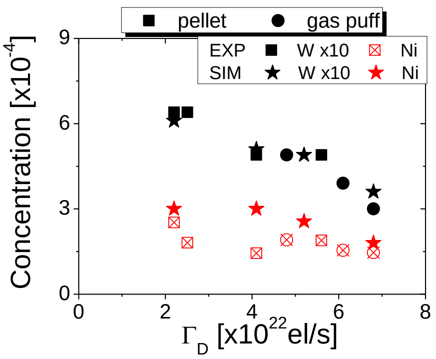

Fig. 4c

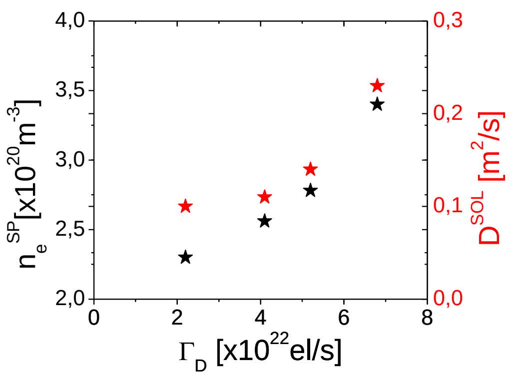

Fig. 4d

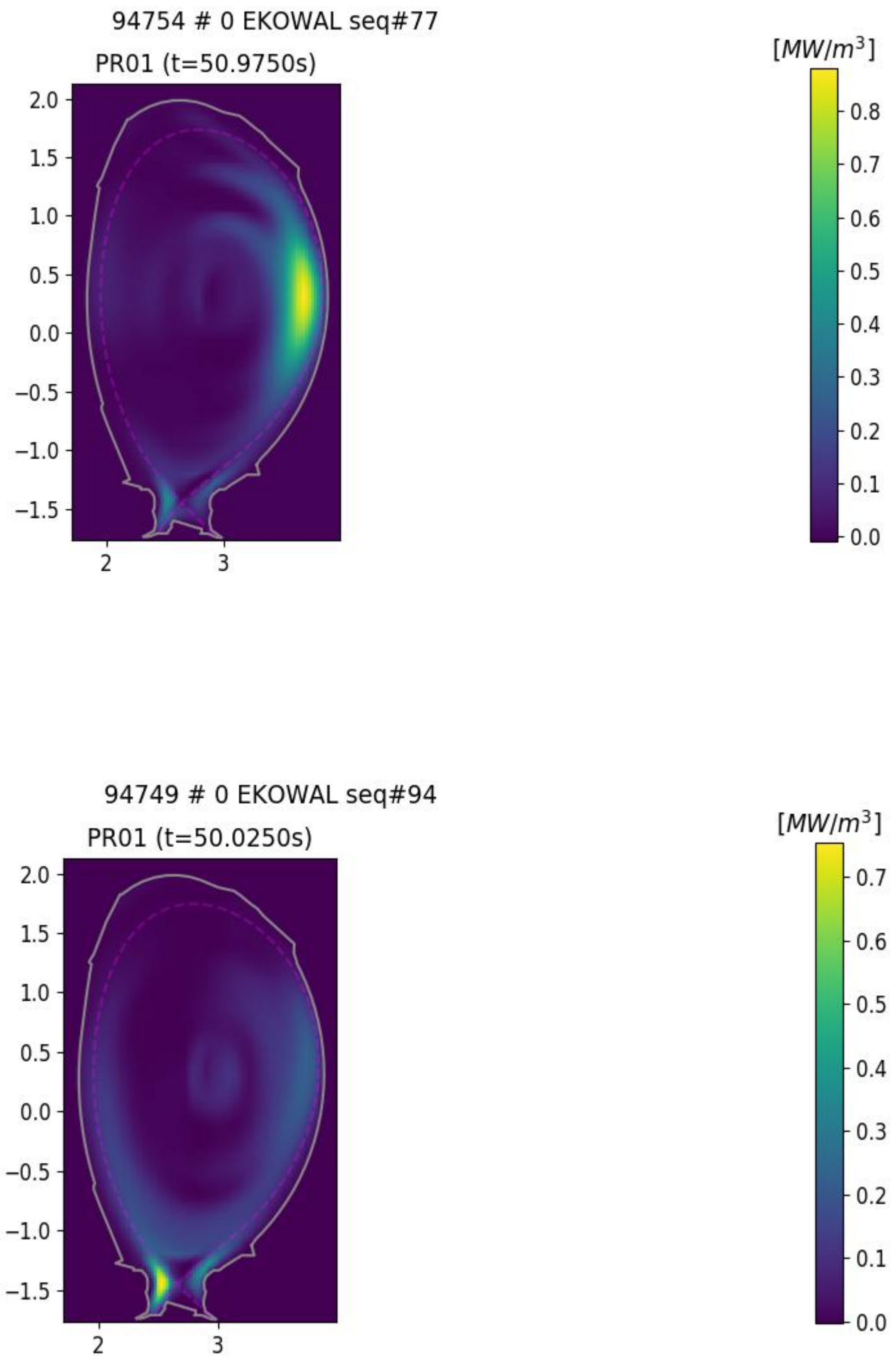

94754 # 0 EKOWAL seq#77
PR01 (t=50.9750s)
[MW/m3]
94749 # 0 EKOWAL seq#94
PR01 (t=50.0250s)
[MW/m3]

Fig. 5

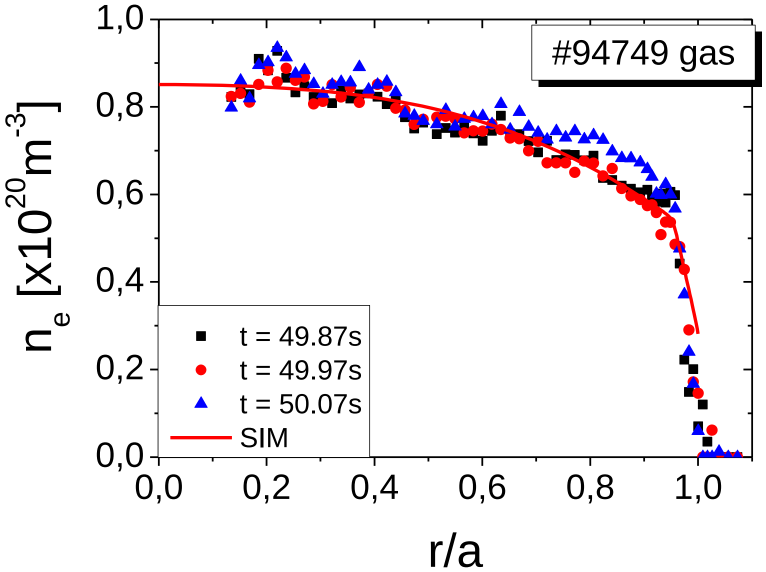

#94749 gas
t = 49.87s
t = 49.97s
t = 50.07s
SIM
n_e [x10^{20}m^{-3}]
r/a

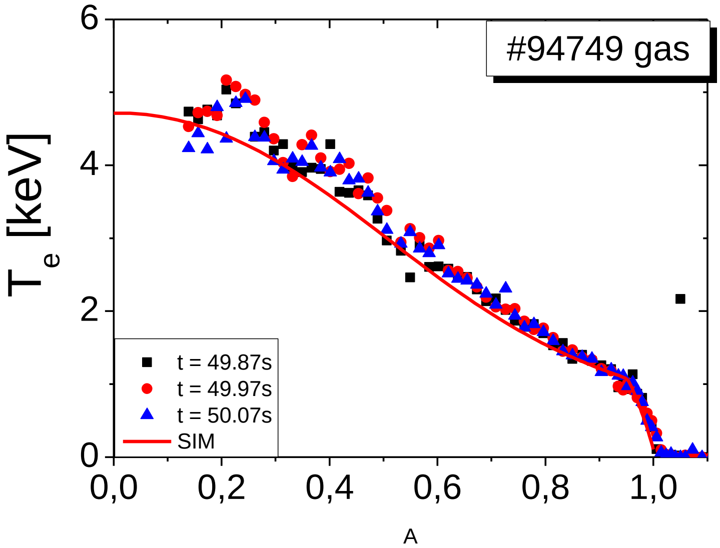

#94749 gas
t = 49.87s
t = 49.97s
t = 50.07s
SIM
T_e [keV]
A

Fig 6 a

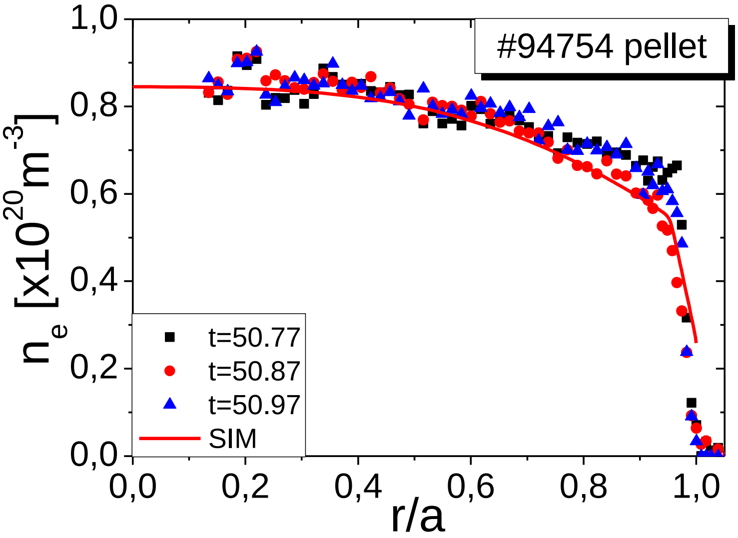

#94754 pellet
n_e [x10^{20}m^{-3}]
r/a
t=50.77
t=50.87
t=50.97
SIM

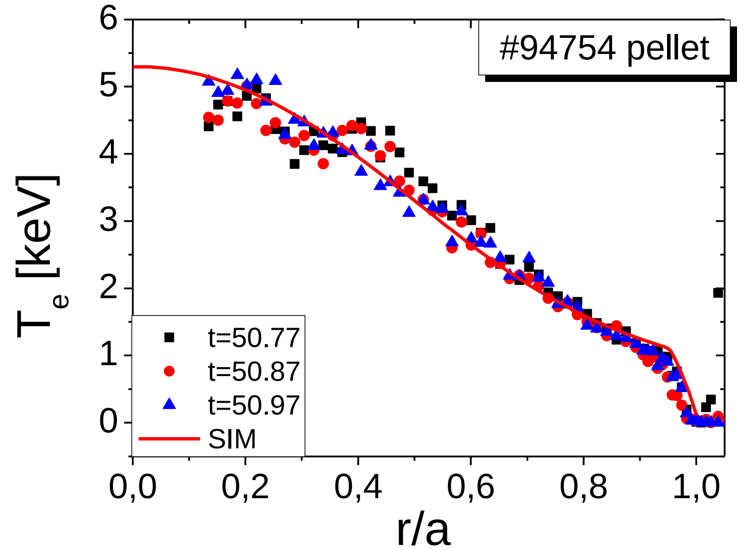

#94754 pellet
T_e [keV]
r/a
t=50.77
t=50.87
t=50.97
SIM

Fig 6 b

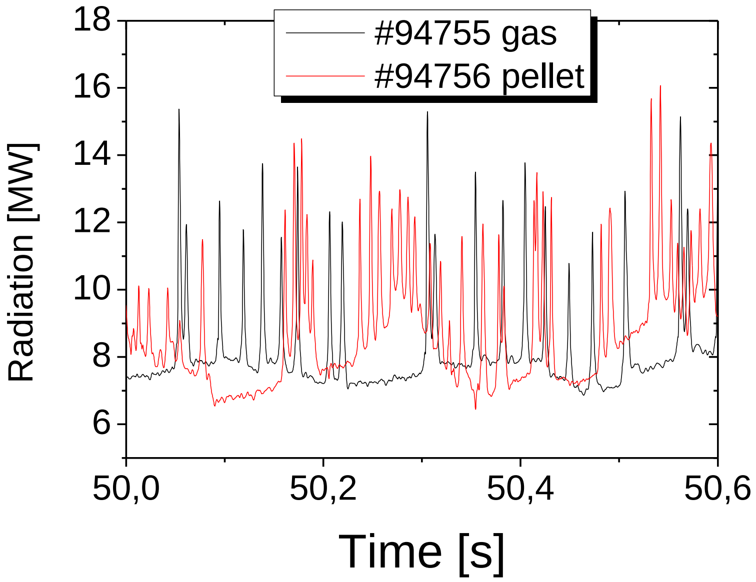
#94755 gas
#94756 pellet
18
16
14
12
10
8
6
Radiation [MW]
50,0
50,2
50,4
50,6
Time [s]

Fig. 7

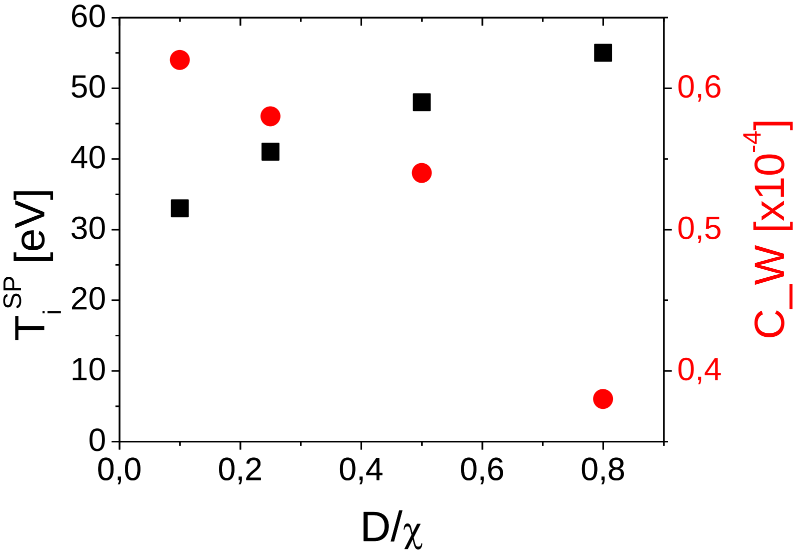

Fig . 8

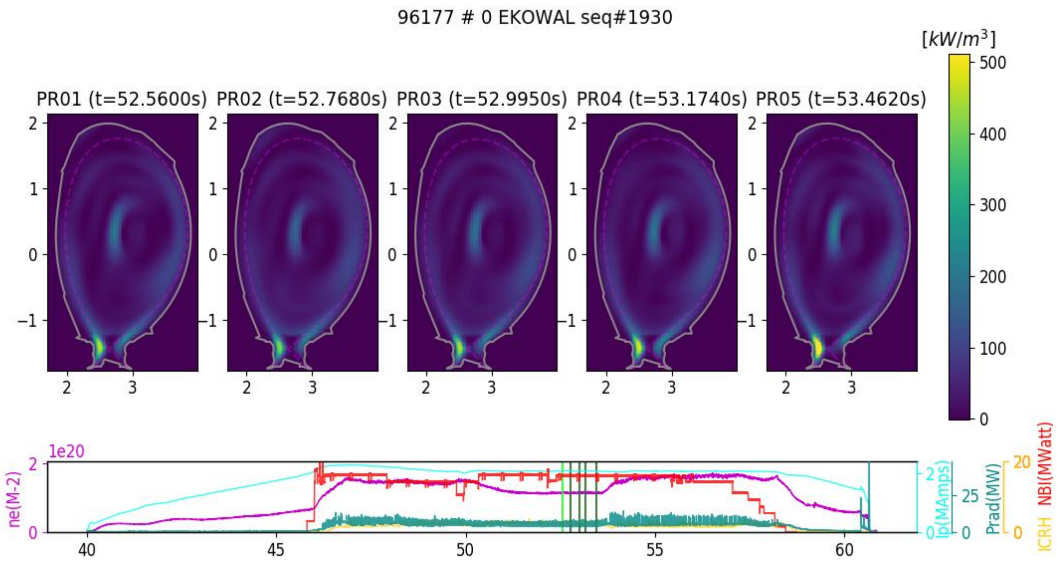

96177 # 0 EKOWAL seq#1930
[kW/m^3]
PR01 (t=52.5600s)
PR02 (t=52.7680s)
PR03 (t=52.9950s)
PR04 (t=53.1740s)
PR05 (t=53.4620s)
1e20
ne(M-2)
Ip(MAmps)
Prad(MW)
ICRH
NBI(MWatt)

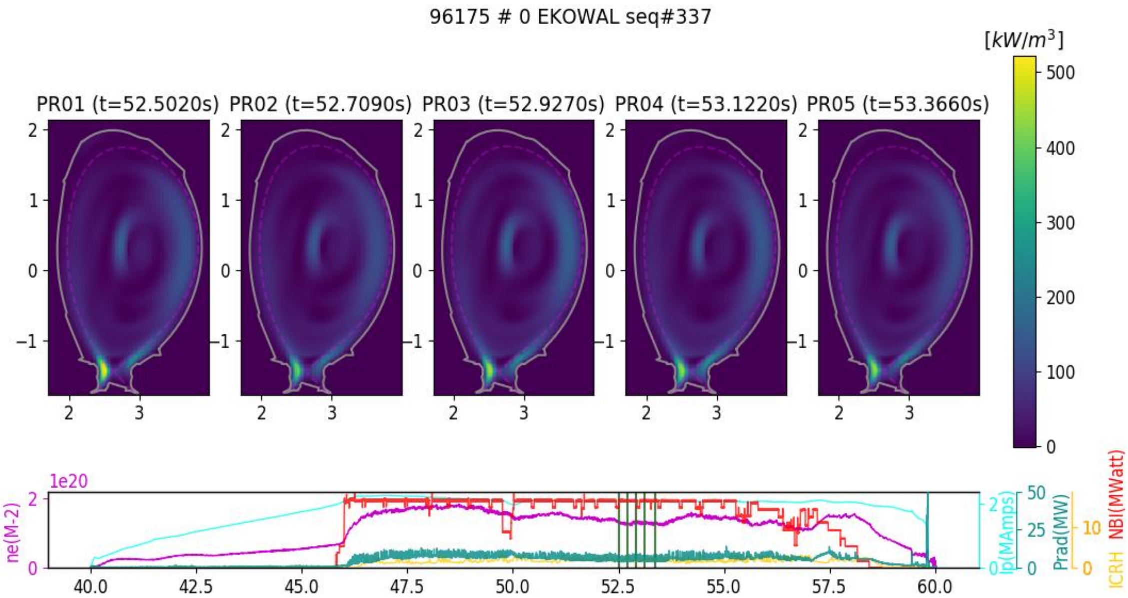

96175 # 0 EKOWAL seq#337
[kW/m^3]
PR01 (t=52.5020s)
PR02 (t=52.7090s)
PR03 (t=52.9270s)
PR04 (t=53.1220s)
PR05 (t=53.3660s)
1e20
ne(M-2)
Ip(MAmps)
Prad(MW)
ICRH
NBI(MWatt)

Fig. 9

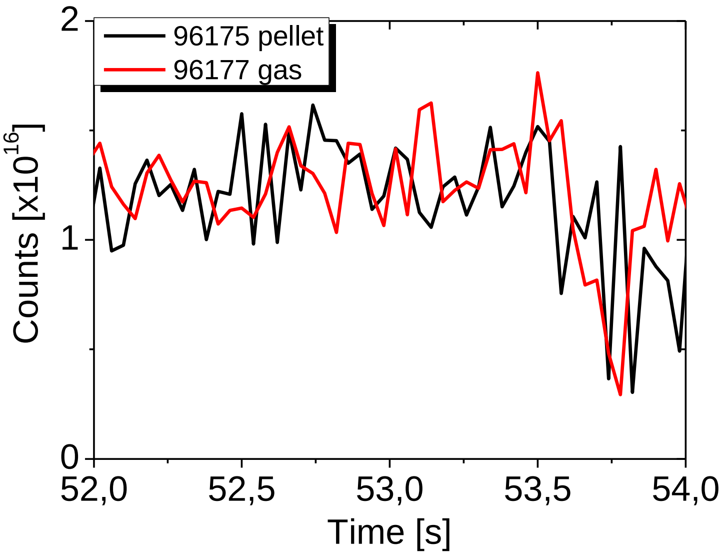

96175 pellet
96177 gas
Counts [x10^16]
2
1
0
52,0
52,5
53,0
53,5
54,0
Time [s]

Fig. 10